AD

AD-E400 144

TECHNICAL REPORT ARLCD-TR-78013

DYNAMIC ANALYSIS OF THE XM650E4 8-INCH PROJECTILE

BRUCE KNUTELSKY

APRIL 1978

US ARMY ARMAMENT RESEARCH AND DEVELOPMENT COMMAND
LARGE CALIBER
WEAPON SYSTEMS LABORATORY
DOVER, NEW JERSEY

The findings in this report are not to be construed as an official Department of the Army position.

DISPOSITION

Destroy this report when no longer needed. Do not return to the originator.

REPORT DOCUMENTATION PAGE

READ INSTRUCTIONS BEFORE COMPLETING FORM

1. REPORT NUMBER: Technical Report ARLCD-TR-78013
2. GOVT ACCESSION NO.:
3. RECIPIENT'S CATALOG NUMBER:

4. TITLE (and Subtitle): DYNAMIC ANALYSIS OF THE XM650E4 8-INCH PROJECTILE

5. TYPE OF REPORT & PERIOD COVERED:

6. PERFORMING ORG. REPORT NUMBER:

7. AUTHOR(s): Bruce Knutelsky

8. CONTRACT OR GRANT NUMBER(s):

9. PERFORMING ORGANIZATION NAME AND ADDRESS:
ARRADCOM
Applied Sciences Division
Dover, NJ 07801

10. PROGRAM ELEMENT, PROJECT, TASK AREA & WORK UNIT NUMBERS:

11. CONTROLLING OFFICE NAME AND ADDRESS:
ARRADCOM
ATTN: DRDAR-TSS
Dover, NJ 07801

12. REPORT DATE: April 1978

13. NUMBER OF PAGES: 41

14. MONITORING AGENCY NAME & ADDRESS (if different from Controlling Office):
ARRADCOM
Applied Sciences Division
Dover, NJ 07801

15. SECURITY CLASS. (of this report): Unclassified

15a. DECLASSIFICATION/DOWNGRADING SCHEDULE:

16. DISTRIBUTION STATEMENT (of this Report):

Approved for public release, distribution unlimited.

17. DISTRIBUTION STATEMENT (of the abstract entered in Block 20, if different from Report):

18. SUPPLEMENTARY NOTES:

19. KEY WORDS (Continue on reverse side if necessary and identify by block number):

XM650E4 projectile	NONSAP
Dynamic analysis	Finite element
Fast fourier transform	Eigenvalues
Frequency content	Direct integration

20. ABSTRACT (Continue on reverse side if necessary and identify by block number):

A linear dynamic analysis of the XM650E4 8-inch projectile is obtained under a gun-launched environment. The chamber pressure, generating projectile motion, is examined for frequency content by a Fourier transform method. The response characteristics of the projectile are determined from a solution to the general eigenvalue problem. The finite element computer code, NONSAP, is utilized to solve the incremental equations of dynamic equilibrium by a direct integration

20. ABSTRACT (Continued)

method. A time-dependent representation of the solution is generated during projectile motion and demonstrates characteristics similar to results of available experimental data. The analysis also determined the response of the projectile to loading conditions approximating the sudden release of forces at muzzle exit.

TABLE OF CONTENTS

INTRODUCTION

The capability of Army analysts to evaluate the structural behavior of projectiles during in-bore motion has closely paralleled the evolution of new numerical methods. Prior to the availability of large core, high speed computers, stress distributions in projectiles were obtained at interfaces of neighboring sections by matching known analytical solutions of standard geometric shapes. The method was limited to only a few sections (Ref 1), and often resulted in conservatively high discontinuous stresses at the intersections. Artillery shells tended to be overdesigned because of the above-mentioned shortcomings of the method. On the other hand, a smooth transition at geometry changes and more realistic distribution of stresses were obtained throughout the projectile body by using the finite element method to solve the linear equations representing quasi-static equilibrium (Ref 2). The designer and analyst were then able to interact more closely to satisfy weight and size limitations and still develop projectiles with peak stresses below the yield strength of the materials.

Designs became more complex with the advent of higher load carrying capacities and weight limitations more severe. As a result, components involved tended to exhibit stresses in the plastic range. By this time, the analytical methods incorporating incremental plastic theory had been inserted into finite element computer codes. Solutions utilizing these methods demonstrated that in most cases the high projectile stresses were not catastrophic in nature and were usually confined to small regions of localized plastic deformation (Ref 3).

Paralleling the development of incremental plastic techniques, finite element methods were being formulated to solve the linear equations of dynamic equilibrium. The conventional method of solution is to use a process based on normal mode superposition as opposed to direct integration. However, this approach, limited to linear systems, is economically restricted to structures where only a few modes of vibration are excited and offers no alternatives. The more versatile method then is to solve the linear dynamic system by direct integration (Ref 4). This linear formulation has been applied to such Army related areas as determining the effects of dynamic forces on projectiles or gun tubes as well as calculating the responses of structures to blast or earthquakes. More important, the formulation could be expanded to include material and geometric nonlinearities. The nonlinear representations of the equations of motions are contained in the computer code, NONSAP (Ref 5). This code is ideally suited to solve most of the structural problems of in-bore dynamics.

FORMULATION

The XM650E4 8-inch rocket assisted projectile (Fig 1), is analyzed as a two-dimensional continuum, but is numerically partitioned into nine distinct regions of different material properties. The actual densities of the nine sections are slightly altered to match independently calculated geometric properties. The material composition and yield strength of the four major structural regions are presented in Table 1.

Table 1
XM650E4 material properties

Section	Material	Yield strength
Motor Body	4340 steel	1250 MPa
Warhead	HF1 steel	1000 MPa
Ogive	7075-T6 aluminum	500 MPa
M739 PD Fuze	2024-T4 aluminum	400 MPa

In anticipation of long-term Army needs, NONSAP was selected for its nonlinear capabilities. However, in this analysis only the linear material property options are utilized to solve the governing equations of dynamic equilibrium. The numerical solution is obtained at the nodes of the discrete set of structural elements (Fig 2). The numerical grid contains 599 node points and 166 quadratic elements. The isoparametric element containing eight nodes is used as the basic element. With this formulation a better definition of forces and geometry can be obtained along the curved surfaces of the projectile.

The motion of the projectile in the gun tube is initiated by gas pressure building up in the chamber. After overcoming the resistive force of the rotating band the projectile is propelled down the tube. The gas pressure acts along the outside surface of the motor body up to the band seat, element 16, where it is obturated by the rotating band. The gas pressure-time curve (Fig 3) is a piece-wise linear representation of an analog simulation of the burning characteristics

of a zone 9 propellant at 145°. The curve is constructed from 24 piece-wise linear sections which are more closely spaced in regions of rapidly changing slopes than in smoother portions of the plot. It is assumed that only after a shot start pressure of 7 MPa does the projectile begin to move. A peak gas pressure of 280 MPa occurs at a time of 5.78 msec. After 16.5 msec of travel the projectile exits the gun tube and the gas pressure drops to zero.

The gilding metal rotating band is in continuous contact with the gun tube during the launch of the projectile. The resulting diametral interference generates a radial band of pressure on the two-inch-wide rotating band seat. This band pressure is experimentally monitored by strain gaging the gun tub at various stations along its length. The circumferential strain on the external wall of the tube is recorded as the projectile passes beneath a gage. The same stations of the gun tube are also analyzed by the finite element method under static loading conditions. The magnitude of the band pressure is then taken to be that two-inch cylindrical band of inward directed radial pressure, which, coupled with the known gas pressure, generates identical strains at each station by the two methods of analysis. This procedure results in a relationship between band pressure and distance traveled. The relationship is then converted to a band pressure-time curve (Fig 4) by utilizing the analog generated distance-time traces. The curve is composed of 14 piecewise linear sections. A peak band pressure of 270 MPa occurs at 4.68 msec, which is two milliseconds in advance of the peak in gas pressure.

The band pressures were experimentally determined during tests conducted with low zone pressure and are extrapolated out to the muzzle. No experimental data is available for zone 9 firings. Thus the calculated magnitudes of band pressure ordinates in Figure 4 are likely to be too high. The higher gas pressure of zone 9 will cause greater radial expansion of the tube with the result of relieving the interference between the band and the tube.

A resistive axial force due to friction was applied to the band seat and calculated by assuming a coefficient of friction of 0.08 operating on the band pressure.

One of the objectives of this analysis is to determine what adverse effects, if any, the sudden release of forces at muzzle exit has on the projectile. The magnitudes of the assumed band pressure and gas pressure at exit (Fig 5) are 150 MPa and 40 MPa, respectively. The exact shape of the decay geometry of the exit forces is unknown. It is assumed that the drop-off of pressure occurs in a linear manner, with the band pressure first, followed immediately by the gas pressure.

Based on experimental studies of many different projectiles, it is recognized that after the projectile exits, the gas pressure reduces to zero within one to three calibers of travel. The XM650E4 projectile has an exit velocity for a zone 9 charge of 760 msec. At this rate, the projectile travels one caliber (8 inches) in 270 microseconds.

Two cases of exit times were assumed in order to account for the uncertainties in the release pressures. In Case 1, both the band and gas pressures are assumed to decay in one caliber. For Case 3, the band pressure drop-off distance is taken as 2 inches (the band width) and gas pressure decay of three calibers is assumed. It is believed that the two cases should bracket the true exit condition.

The frequency content of the forcing functions determines which natural modes of the structure will be excited. The frequency spectrum of the pressure-time curve, shown in Figure 6, was obtained by a fast Fourier transform (Ref 6). The magnitude representing the the square root of the sum of squares of the Fourier coefficients is plotted as the logarithm of those values. On a linear scale this same data appears only as a spike. The primary frequency is the steady state component. By using a cut-off scale of 5, which is 0.1% of peak magnitude, the significant frequency content is less than 4000 Hertz. The curve represents a drop-off time of 100 microseconds, as indicated from Figure 3. If a decay of 270 or 810 microseconds were used, corresponding to Figure 5, lower frequencies would have resulted.

The frequency spectrum of the band pressure curve is presented in Figure 7. Once again using the 0.1% criterion, a frequency content of less than 8000 Hertz is obtained for a drop-off time of 60 microseconds. When the inverse Fourier transform is taken of the gas pressure and band pressure spectra, the original curves are obtained (see Fig 3 and 4).

GOVERNING EQUATIONS

The incremental equations satisfying dynamic equilibrium at time t for the element assemblage of Figure 2 are:

$$M \ddot{U}_{n+1} + C \dot{U}_{n+1} + K (U_{n+1} - U_n) = R_{n+1} - F_n$$

where cycle n+1 refers to time $t+\Delta t$; M, C, and K are the mass, damping, and stiffness matrices, respectively; U, $\dot{U}$, and $\ddot{U}$ are nodal point vectors of displacement, velocity, and acceleration, respectively; R is the vector of external loads applies at time $t+\Delta t$; and F is the vector of nodal point forces equivalent to the element stresses at time t. The results of test cases indicated that with quadratic elements a consistent mass matrix formulation is necessary for accuracy. For this analysis the damping matrix will not be used and a constant stiffness matrix is assumed. The radial forces due to spin are inserted as pseudo-forces and added to the vector F_n.

The Newmark step-by-step integration method is utilized to solve the resulting system of equations in an implicit manner. In this method, the solution at the end of a time step is formulated in terms of a Taylor series expansion with the remainder term being expressed by two free parameters of integration as:

$$U_{n+1} = U_n + \Delta t\, \dot{U}_n + \frac{\Delta t^2}{2} \ddot{U}_n + \beta \Delta t^2 \, (\ddot{U}_{n+1} - \ddot{U}_n)$$

$$\dot{U}_{n+1} = \dot{U}_n + \Delta t\, \ddot{U}_n + \gamma \Delta t \, (\ddot{U}_{n+1} - \ddot{U}_n)$$

where β and γ determine the amount of acceleration that contributes to the displacement and velocity at the end of each interval.

The Newmark parameters were modified by Goudreau (Ref 7) to include damping and are expressed for this analysis as:

$$\gamma = 0.50 + \delta$$

$$\beta = 0.25 \, (1 + \delta)^2$$

The resulting scheme is unconditionally stable and represents constant acceleration during a given time interval. It was found by Goudreau, and observed on the 8-inch projectile, that a slight amount of damping, $\delta = 0.05$, will suppress the spurious oscillations that result from the discrete grid representation of the continuum without distorting the dominant characteristics of the system.

The governing equations are then reformulated in terms of incremental displacements and a solution is obtained by conventional matrix methods.

The fundamental frequencies and mode shapes of the element assemblage must be calculated in order to select a suitable time step, Δt, for the incremental solution and to determine the response characteristics of the structure. In NONSAP a determinant search method is used to solve for the eigenvalues and eigenvectors of the system using the relationship

$$M\Phi\Omega^2 - K\Phi = 0$$

In this expression M is the mass matrix, K is the stiffness matrix and Φ is the matrix of eigenvectors which are mass ortho-normalized. Ω^2 is the diagonal matrix of eigenvalues. For this analysis, a lumped mass assumption is made in the eigenvalue routine.

The first ten natural frequencies and associated periods of the structural system (Table 2) are obtained from the calculated eigenvalues.

Table 2
XM650E4 natural frequencies

Mode	Frequency (Hertz)	Period (Microseconds)
1	210	
2	2970	337
3	4010	249
4	5300	189
5	6680	150
6	7250	138
7	7460	134
8	8000	125
9	8280	121
10	9020	111

The corresponding mode shapes are obtained from the eigenvectors and can be evaluated by superimposing the modal displacements on the original grid. The sensitivity of the projectile to the first ten frequencies can then be assessed by comparing the deflected configuration to the original grid. The first mode shape is evaluated in this manner and observed to be the rigid body mode. The non-zero value of the corresponding frequency results from restraining an axial node, the center of gravity, which is necessary in the NONSAP eigenvalue routine. The profile of the projectile after adding the second mode shape (Fig 8) illustrates the extension of the ogive and flexibility of the joint at the forward section of the motor body. The plots are scaled magnifications of the deflected configurations and are determined for mass-normalized peak amplitudes. The third and fourth mode shapes also demonstrate similar flexible features. The fifth mode shows that the principal vibratory response is in the boat tail. The last five modes illustrate the formation of higher order waves along the length of the projectile.

An incremental time step, Δt, for the step-by-step solution can be obtained by using the criterion

$$\frac{\Delta t}{T} \leq 0.1$$

where T is the period of the highest frequency that may be accurately included in the solution. The regulating criterion of the integration scheme implies that contributions from the remaining modes decrease as the corresponding frequencies increase. By selecting a time step of 10 microseconds, all of the response characteristics of the first 10 mode shapes are included in the analysis with a minimum of error.

ANALYSIS

For the initial phase of the analysis, a dynamic solution of the XM650E4 projectile is obtained under loading conditions corresponding to Case 1 (Fig 5) in which it is assumed the pressures drop off in 270 microseconds. The dynamic analysis by direct integration solves the equations of motion for each of the 599 node points in the structure for 2000 cycles at a time step of 10 microseconds. During the time-dependent solution 16 node points and 17 elements are continuously monitored in order to display the total displacements, velocities, accelerations, and stresses. The variables of motion for a characteristic point in the fuze, node point 585, are illustrated in Figure 9. The acceleration exhibits a small amplitude oscillation, but generally follows the pressure-time curve throughout the 16.5 milliseconds of travel and shows a sudden increase in amplitude to 3000 G's at muzzle exit. Oscillations with these amplitudes should not have any adverse effects on the fuze structure or components.

Experimental data for high zone firings are needed to confirm the results. Characteristics of motion similar to those in Figure 9 were recently obtained by Gary Bubb of Picatinny Arsenal from low zone experimental tests of the XM650E4 8-inch projectile (Fig 10). Except for the initial aspects of acceleration, there is a noticeable similarity in the traces until information is lost at muzzle exit. The decay in the experimental acceleration at 8 milliseconds is due to the high resistive forces which are generated during the engraving of the rotating band. There is currently no obvious analytical formulation that can easily be coupled to the finite element solution to describe this particular phase of motion. The attempt in the analysis to include the frictional forces as a function of band pressure did not duplicate the acceleration dip but merely generated periodic agreement with the standard analog simulation of velocity and distance values.

The instrumentation in the experimental test of the low zone firings consisted of piezo-resistive pressure gages situated in the gun chamber and piezo-resistive accelerometers mounted in the ogive of the projectile. Information is transferred by hard wires to recording devices with a 20,000 Hertz frequency response. Data is lost when the collecting cup (used to retrieve the wiring) exits the muzzle and breaks the wires, thus ending information. The distances and velocity curves are generated by assuming rigid body motion and integrating the unfiltered accelerometer data. The lower gas pressure causes all of the variables of motion to be considerably less than those calculated for the zone 9 charge. The details of the experimental technique and the data reduction methods used on a 155MM projectile test are presented in Reference 8.

The curves representing axial motion for a node point in the boat tail, node number 3, generated under the same loading condition (Case 1), shows little oscillation in the acceleration (Fig 11). The drop-off of acceleration at muzzle exit reveals only small amplitudes. This smooth behavior of the boat tail can be explained by recalling that the first ten modes of vibration of the projectile indicated very little sensitivity of the boat tail to the low order frequency content of the applied gas pressure. The initial oscillations are caused either by the shot start pressure or by numerical error generated by not obtaining complete equilibrium at the first movement of the projectile.

The curves representing motion for the node points in the fuze and boat tail are characteristic values for the entire structure. Values plotted for the remaining monitored node points reveal magnitudes of oscillation that lie between the two. In all cases the velocity and distance curves were quite smooth, being integral plots of the acceleration. The computer time for the complete solution of 20 milliseconds was approximately one hour of CDC 6600 central processor time. This time should not be used as a benchmark for NONSAP, for it included the time-consuming options that were inserted to calculate spin forces as a function of changing velocity and to interpret stress contours at extra boundary integration points. The Tektronix 4014 storage tube graphics system was used to obtain hard copy plots for the evaluation of the solution.

In order to obtain exit characteristics for load Case 3, the solution is restarted at 15 milliseconds and the pressure curves are redefined. The axial acceleration at exit exhibits severe oscillations of a peak magnitude of 7000 G's (Fig 12). It is probable, if these values are realistic, that fuze components cannot withstand these calculated forces and function properly. However, it should be kept in mind that the numerical solution can only reflect the response of the fuze to the assumed forcing function. The accelerations of the other monitored points show higher magnitudes for this case than for Case 1, but none as severe as those points in the fuze.

The large amplitudes of the load of Case 3 are caused by the 67-microsecond drop-off of the resistive force. The magnitude of the resistive force at projectile exit is controlled by the high value of band pressure and the assumed value of the coefficient of friction. In recent studies (Ref 9) it is shown that after a high coefficient of friction during engraving, a hydrodynamic film on the rotating band causes the coefficient of friction to drop to 0.02 at projectile exit. The low value is generated because of high velocity and bearing pressure.

The magnitudes of the axial and radial stresses for the element under the rotating band, element 16, are presented in Figures 13 and 14, respectively. The smooth axial stress values follow the shape of the pressure-time curve which generates axial acceleration. The radial stress shape is quite similar to the band pressure-time curve. These stresses represent the maximum stressed region in the projectile and are below the yield strength of 4340 steel. The magnitude of these stresses in the other monitored elements also indicates stress values well below the material yield strengths. The monitored components consisted of the radial, axial, circumferential, and shear stresses. Although the acceleration values indicate oscillations, the corresponding curves representing the stress components were quite smooth.

The radial displacement of the node under the rotating band, node 89, as a function of time exhibits the combined effects of gas and band pressure (Fig 15). For the first 5 milliseconds the radial deformation is dominated by the band pressure. Between 5 and 8 milliseconds the band forces decrease and the radial forces of gas pressure prevail. After 8 milliseconds the influence of the band pressure returns. At muzzle exit the deformations become positive due to the high velocity and spin forces. Experimental tests, using strain gages in the circumferential direction mounted under the rotating band, exhibit similar characteristics.

The curves all demonstrate that a static equilibrium approach is valid for projectile analysis if equilibrium is satisfied at a specific time such as peak pressure. Of course, this is valid if dynamic forces such as muzzle exit conditions are not applied to the structure. The advantage of an equilibrium analysis lies in the fact that it permits each of the original nine distinct regions to be evaluated separately. The capacity of the computer can then be used to fine grid each section for a more accurate analysis of the stress distribution in that section. More importantly a static solution need only be obtained for one cycle of time.

During the numerical solution, computer dumps are available of all calculated parameters corresponding to such physically relevant conditions as peak band pressure, peak gas pressure, or at muzzle exit. The deflected configuration of the projectile is obtained by superimposing magnifications of the displacements on the original grid. The exaggerated profile at peak gas pressure (Fig 16) illustrates the reaction of the projectile to high acceleration forces. Due to these high forces the overall effect is reflected in a shortening of the projectile around the center of gravity as the base is pushed forward and the ogive sets back. The distortion of the motor body is a direct

result of gas and band pressures being applied to the surface. The deformations are shown to an exaggerated scale. This causes neighboring sections to appear to cross, when in reality they do not.

The stress distribution in the motor body at peak gas pressure (Fig 17) illustrates a complex pattern of interacting stresses. At the corresponding time of 6.78 milliseconds the band pressure has dropped to 210 MPa. The plotted contours are shown for the combined stress, which can be compared to the yield strength of 4340 steel to determine the integrity of the projectile. The highest values of 700 MPa are in the filler radius and forward section and are below the yield strength of 1250 MPa.

The combined stress contours for the warhead, ogive, and fuze are represented in Figures 18, 19, and 20. The corresponding yield strengths are presented in Table 1. The stress distributions demonstrate values well within the elastic range. Stress contours evaluated at peak band pressure and muzzle exit were also low.

CONCLUSIONS

The structural analysis of the XM650E4 8-inch projectile demonstrated an efficient numerical procedure for defining the dynamic characteristics of artillery shells during in-bore motion. The frequency spectra of gas pressure and band pressure were generated through Fourier transform methods and indicated predominantly low frequencies in the forcing functions. A solution of the general eigenvalue problem to obtain natural frequencies and mode shapes illustrated that the ogive portion of the projectile is responsive to these frequencies. A solution to the linear equations of dynamic equilibrium by direct integration shows that the stress distribution in the projectile throughout in-bore travel is below the yield strength of the sectional materials. The numerically determined accelerations at points in the fuze illustrate oscillatory characteristics which are similar to experimentally obtained accelerations. It was demonstrated that there were no adverse effects on the projectile due to the sudden release of gas pressure at muzzle exit. However, on the other hand the calculations indicate that the assumed large magnitude and short drop-off times of the band pressure would result in high acceleration forces at exit. The response of the projectile to dynamic in-bore forces demonstrated that standard static equilibrium solutions are valid at peak pressures.

COMMENTS

The accuracy of the simulation of in-bore motion of the XM650E4 8-inch projectile is dependent on the accuracy of the assumptions that describe the boundary conditions. Experimental tests conducted at high zone gas pressure are necessary to independently verify acceleration values calculated for the projectile during travel. A valid shape of the gas and band pressure curves at muzzle exit must be obtained in order to justify the numerical conclusions.

A frequency spectrum analysis of the gas pressure traces of irregular burning propellant, such as the M2 propellant charge, is a simple method of determining the response of 8-inch rounds. If the significant frequency content is less than 4000 Hertz, no adverse effects will result and further analyses are not necessary.

The capabilities contained in NONSAP offer a wide variety of solutions to the problems associated with in-bore dynamics. The method is capable of handling one-, two-, or three-dimensional structures; linear or nonlinear geometric and material properties; as well as static and dynamic analyses. An updated version of the code, ADINA, eliminates many of the technical difficulties and is more user oriented (Ref 10). The Picatinny pre-processor and post-processor for two-dimensional problems also reduces user evaluation time for NONSAP.

The advantages in using the implicit formulation of NONSAP to solve dynamic problems in which material and geometric nonlinearities are important are uncertain. An explicit formulation, in which the Newmark parameters are set to zero, is a pleasing alternative for the large deformation problems of blast, impact, and penetration (Ref 11). In both formulations a small time step is necessary for long periods of time. However, the explicit scheme sacrifices the accuracy of using the stiffness matrix to satisfy equilibrium for the speed and smaller core requirements of using pseudo-forces to calculate accelerations.

REFERENCES

1. Larson, C. W., Knutelsky, B. G., and Salamon, R. G., "Stress and Deflection Equations for Analyzing Shells with Axially Symmetric Geometry and Loading," Technical Report 3762, Picatinny Arsenal, Dover, NJ, April 1969.

2. Larson, C. W., Knutelsky, B. G., and Salamon, R. G., "Stress Analysis of Shells of Revolution," U. S. Army Munitions Command Science Conference, Picatinny Arsenal, Dover, NJ, June 1969.

3. Knutelsky, B. G., Demitrack, G., and Schwartz, R. M., "Finite Element Stress Analysis of Artillery Projectiles," MS73-95, Society of Manufacturing Engineers, Dearborn, Michigan, October 1973.

4. Bathe, K. J., Wilson, E. L., and Peterson, F. E., "SAP IV - A Structural Analysis Program for Static and Dynamic Response of Linear Systems," EERC 73-11, University of California, Berkeley, California, June 1973.

5. Bathe, K. J., Wilson, E. L., and Iding, R. H., "NONSAP - A Structural Analysis Program for Static and Dynamic Response of Non-Linear Systems," UC SESM 74-3, University of California, Berkeley, California, February 1974.

6. Schiesser, W. E., "FFT-Fast Fourier Transforms," Lehigh University Computing Center Library No. G60001, Bethlehem, Pennsylvania, July 1970.

7. Goudreau, G. L., "Evaluation of Discrete Methods for the Linear Dynamic Response of Elastic and Viscoelastic Solids," SESM-69-15 (PB-194286), University of California, Berkeley, California, June 1970.

8. Bubb, G., "Determination of In-Bore Resistive Force," Second International Symposium on Ballistics and Warhead Mechanisms, Daytona Beach, Florida, March 1976.

9. Montgomery, R. S., "Surface Melting of Rotating Bands," WVT-TR-75060, Watervliet Arsenal, Watervliet, NY, November 1975.

10. Bathe, K. J., "ADINA - A Finite Element Program for Automatic Dynamic Incremental Non-Linear Analysis," Acoustics and Vibration Laboratory Report 82448-1, Mechanical Engineering Department, M.I.T., September 1975.

11. Johnson, G. R., "Finite Element Analysis for High Velocity Impact," Fuze/Munitions Environment Characterization-Symposium II, U. S. Army Armament Command, Picatinny Arsenal, Dover, NJ, October 1975.

XM650E4 8-INCH PROJECTILE

Fig 1 Longitudinal cross section

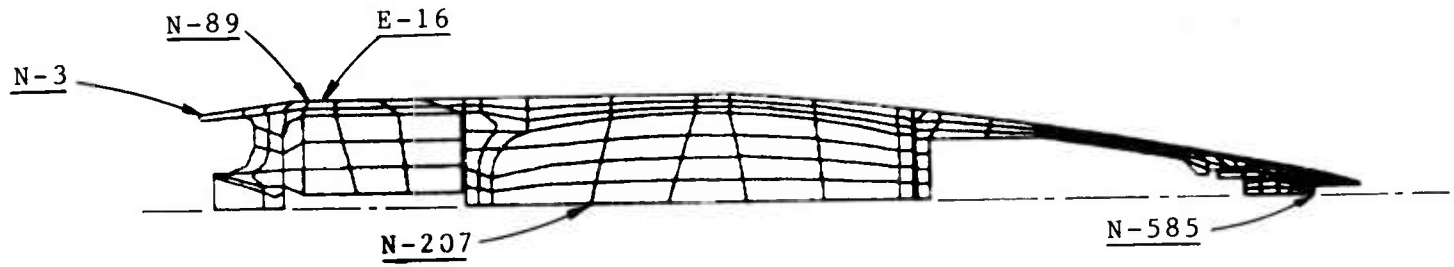

Fig 2 Finite element grid

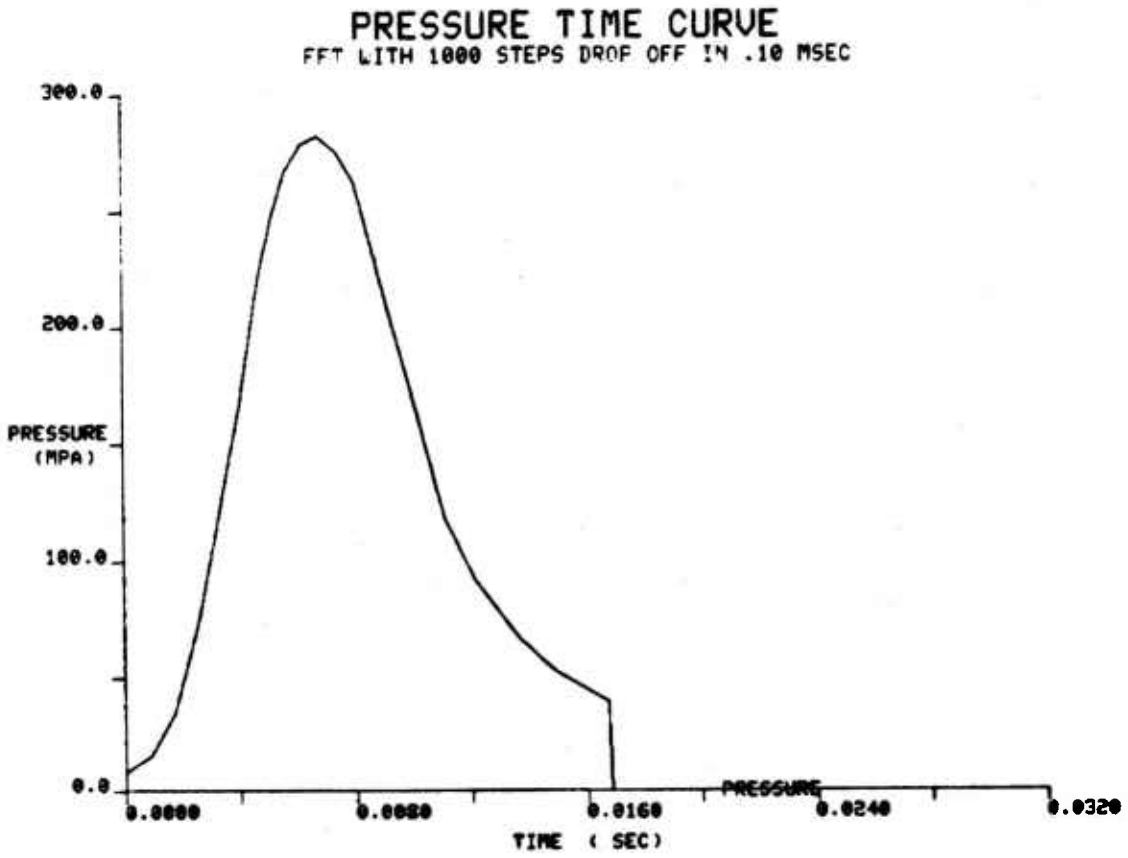

Fig 3 In-bore gas pressure profile (zone 9)

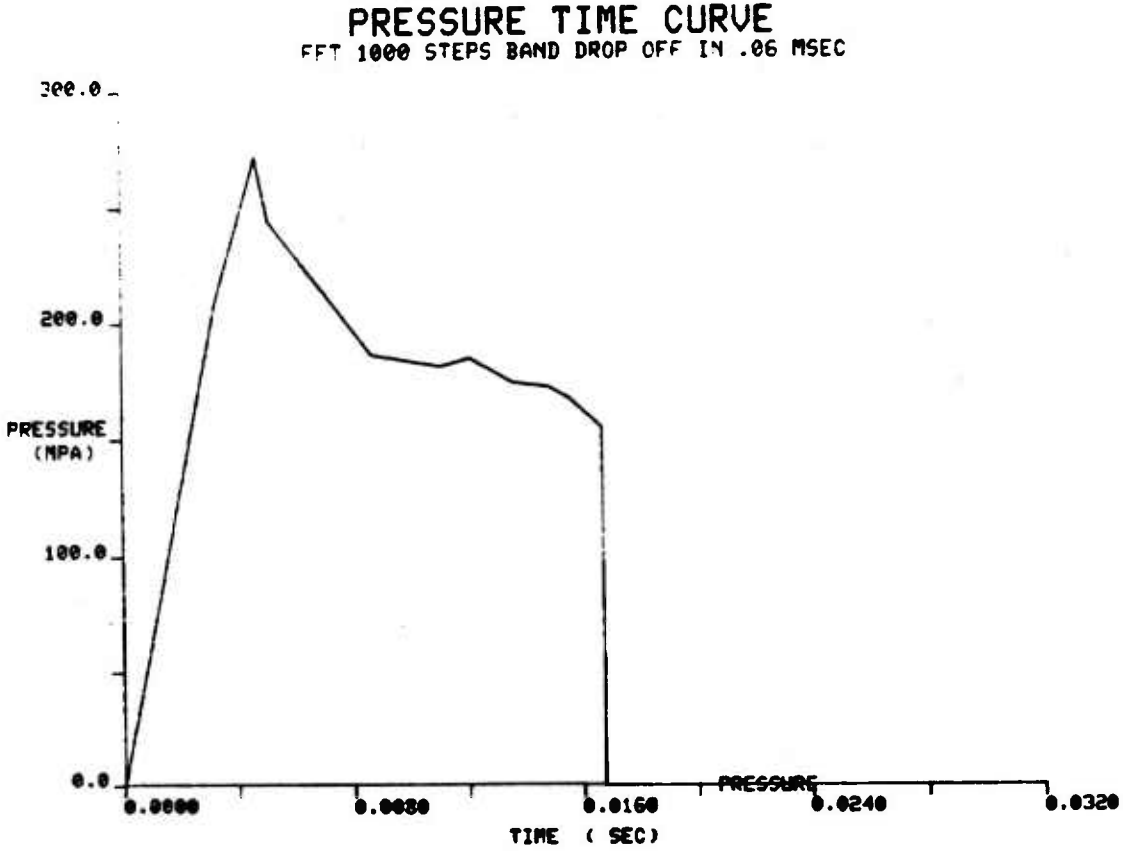

Fig 4 Radial band pressure profile (zone 1)

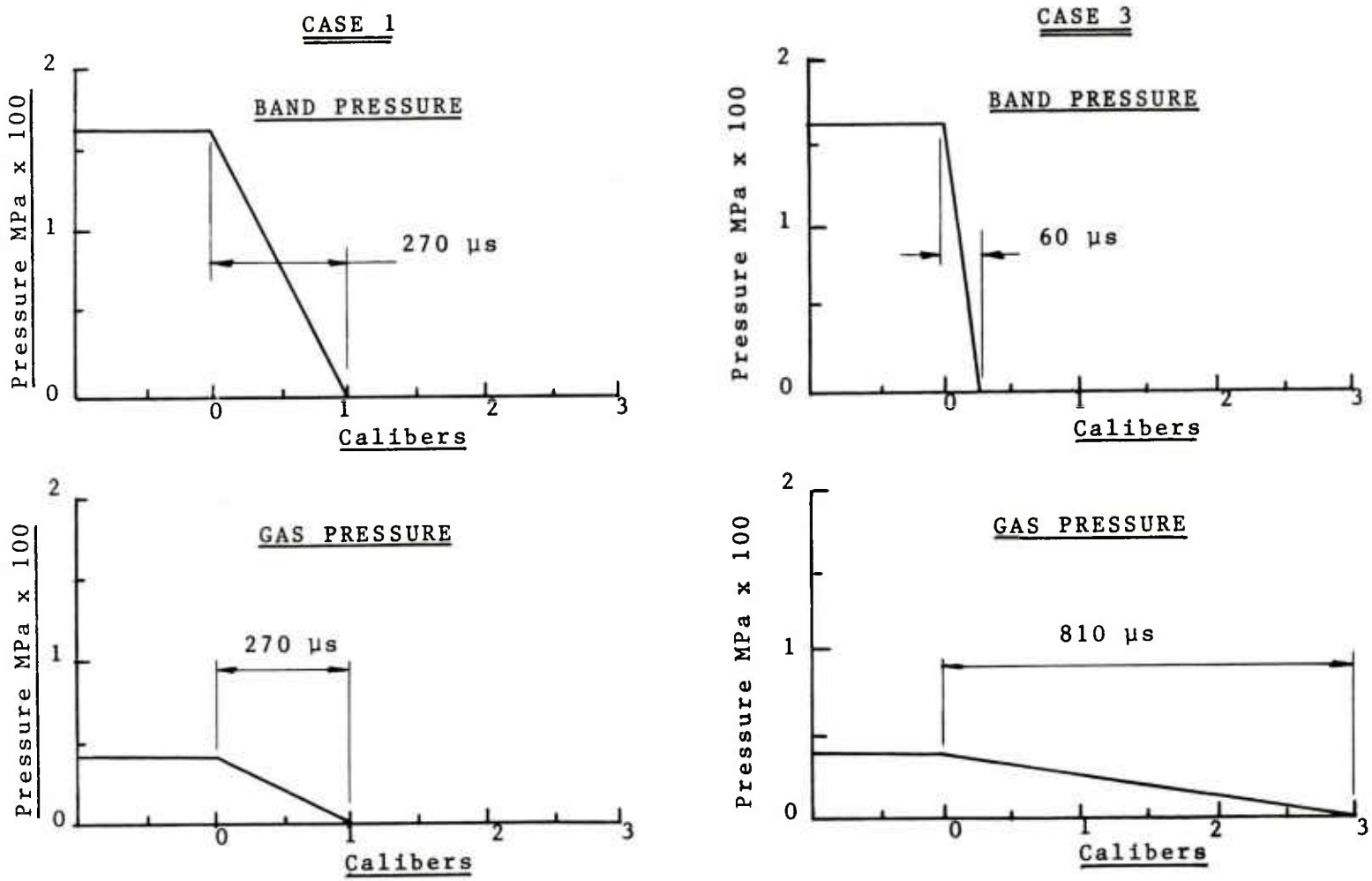

Fig 5 Pressure decay histories

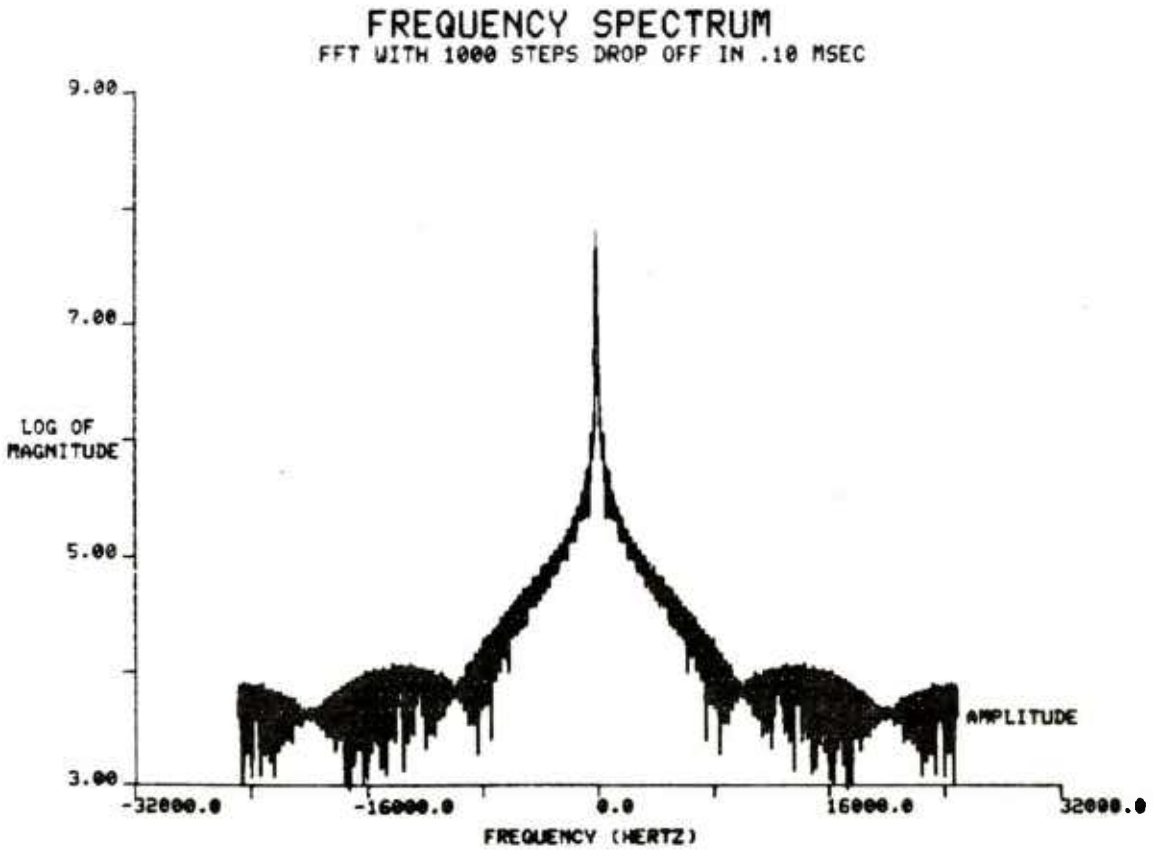

Fig 6 Gas pressure frequency spectrum (MPa)

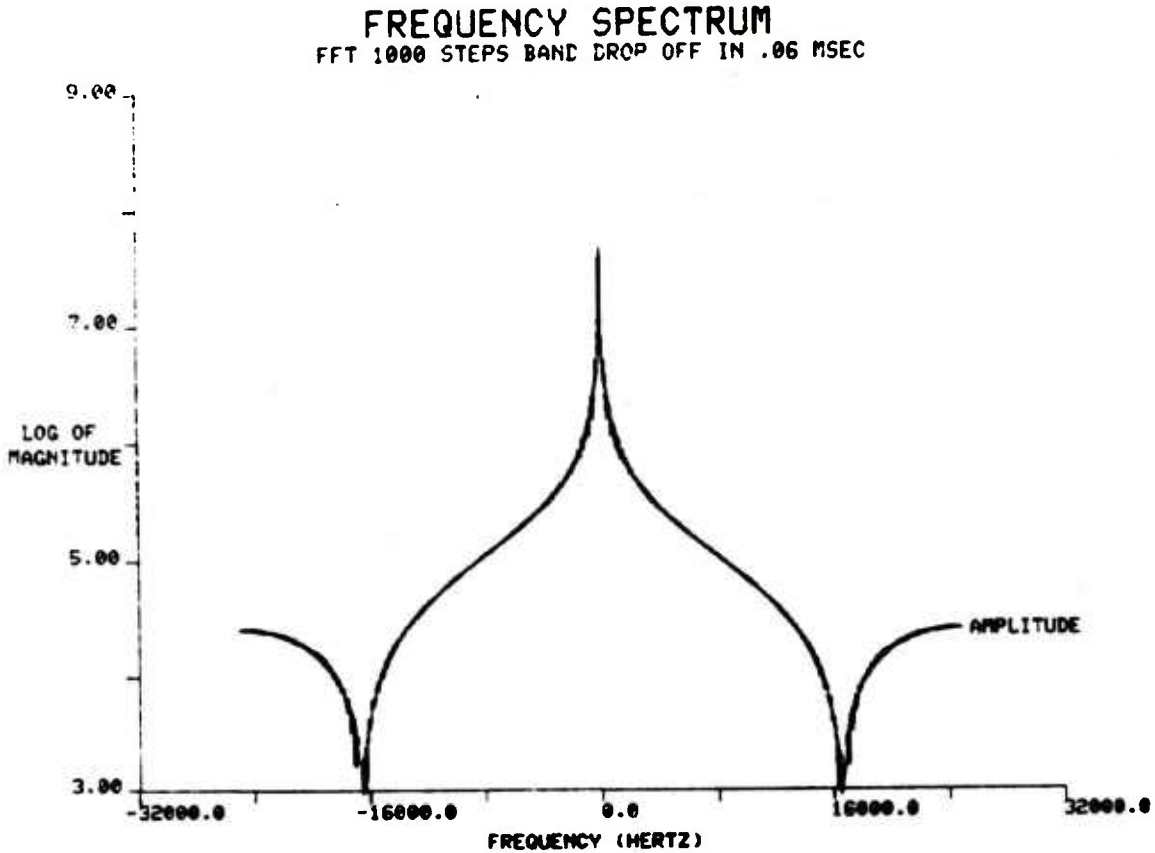

Fig 7 Band pressure frequency spectrum (MPa)

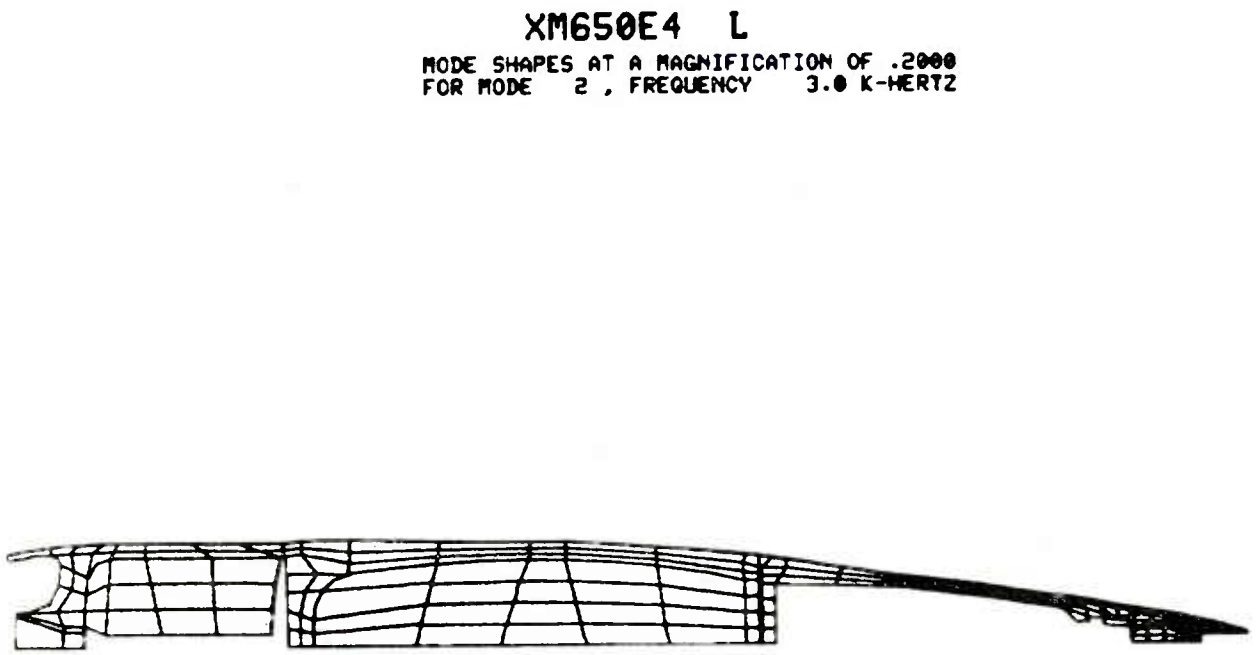

Fig 8 Deflected configuration for mode shape 2

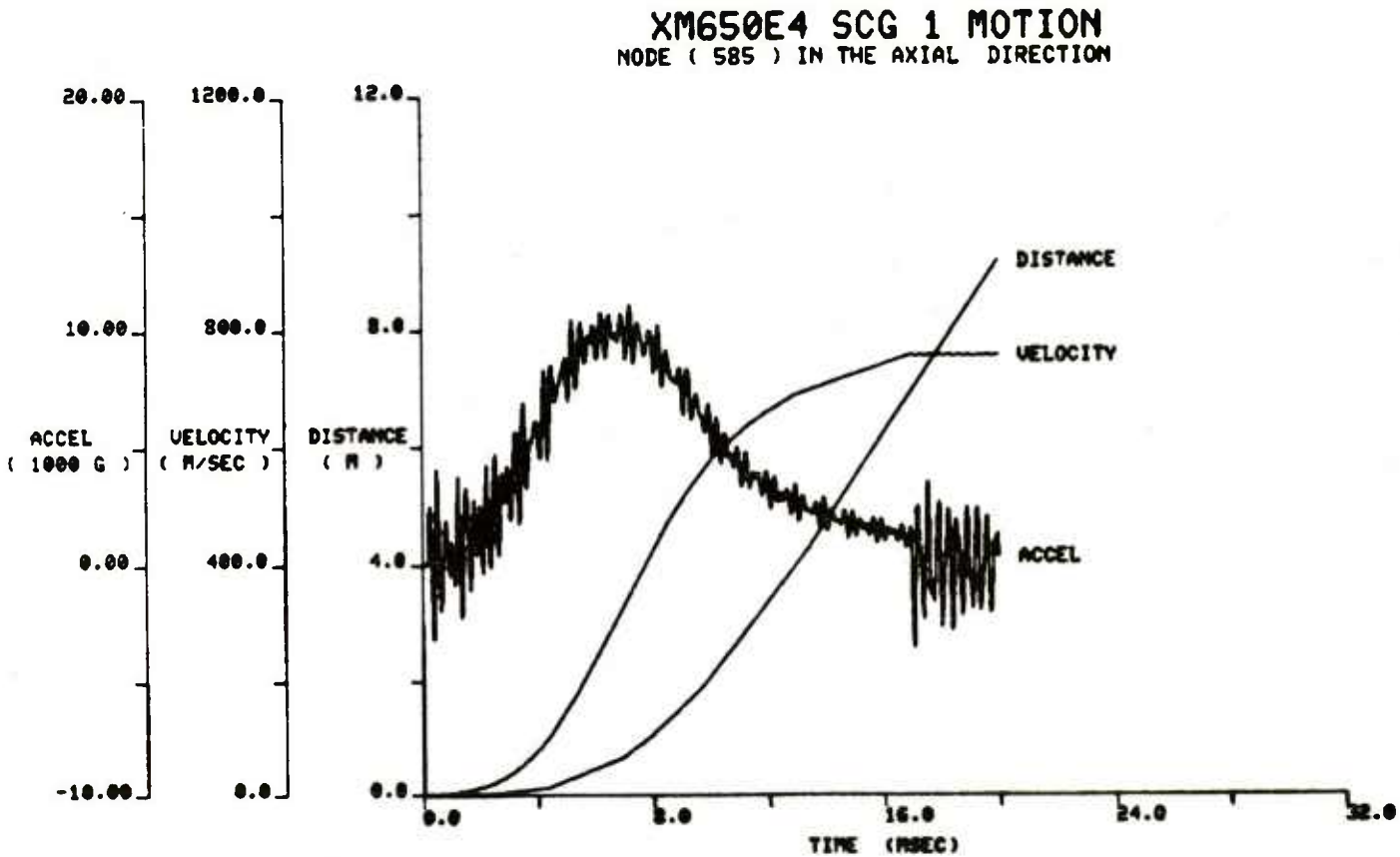

Fig 9 Fuze motion characteristics for Case 1

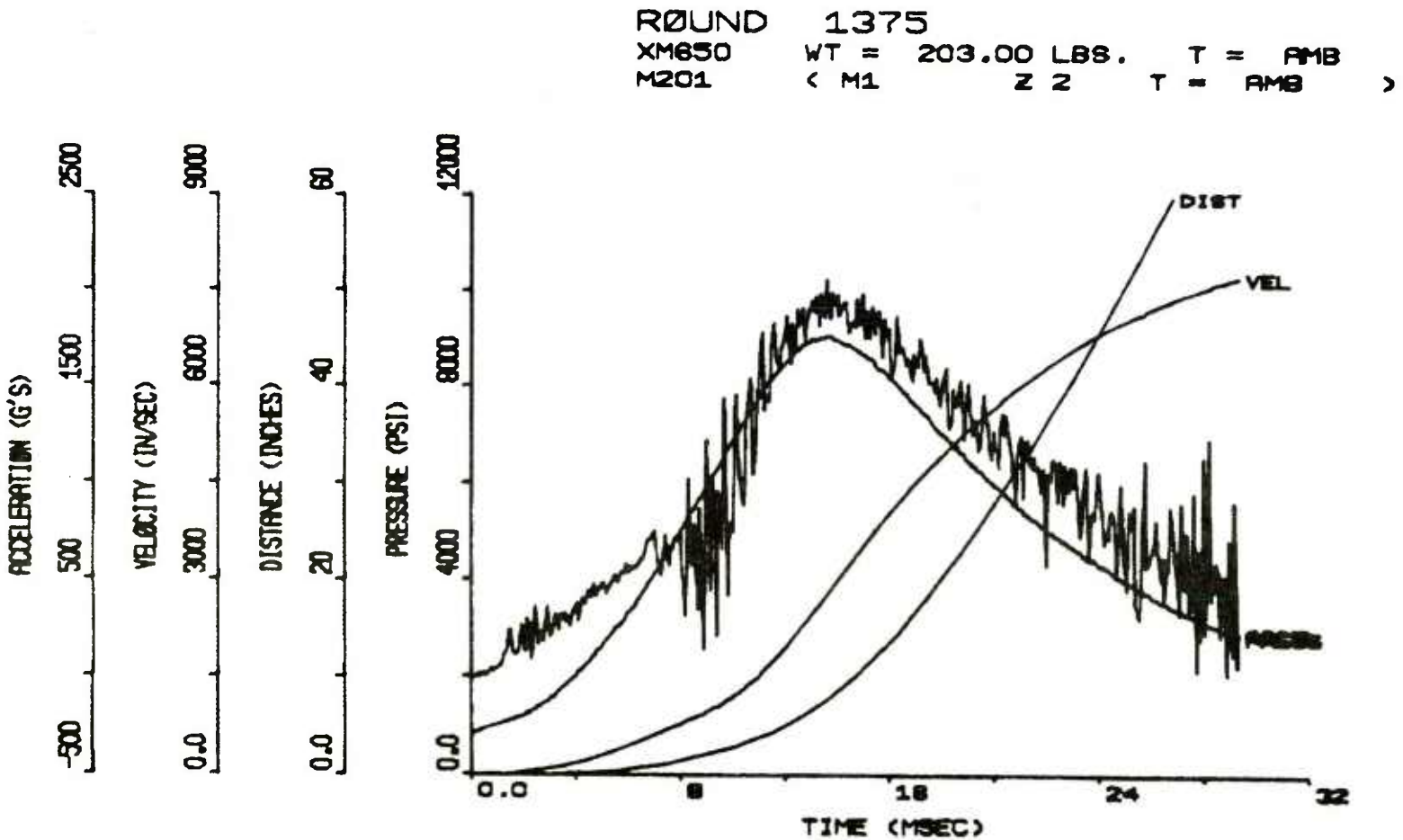

Fig 10 Experimentally determined variables of motion

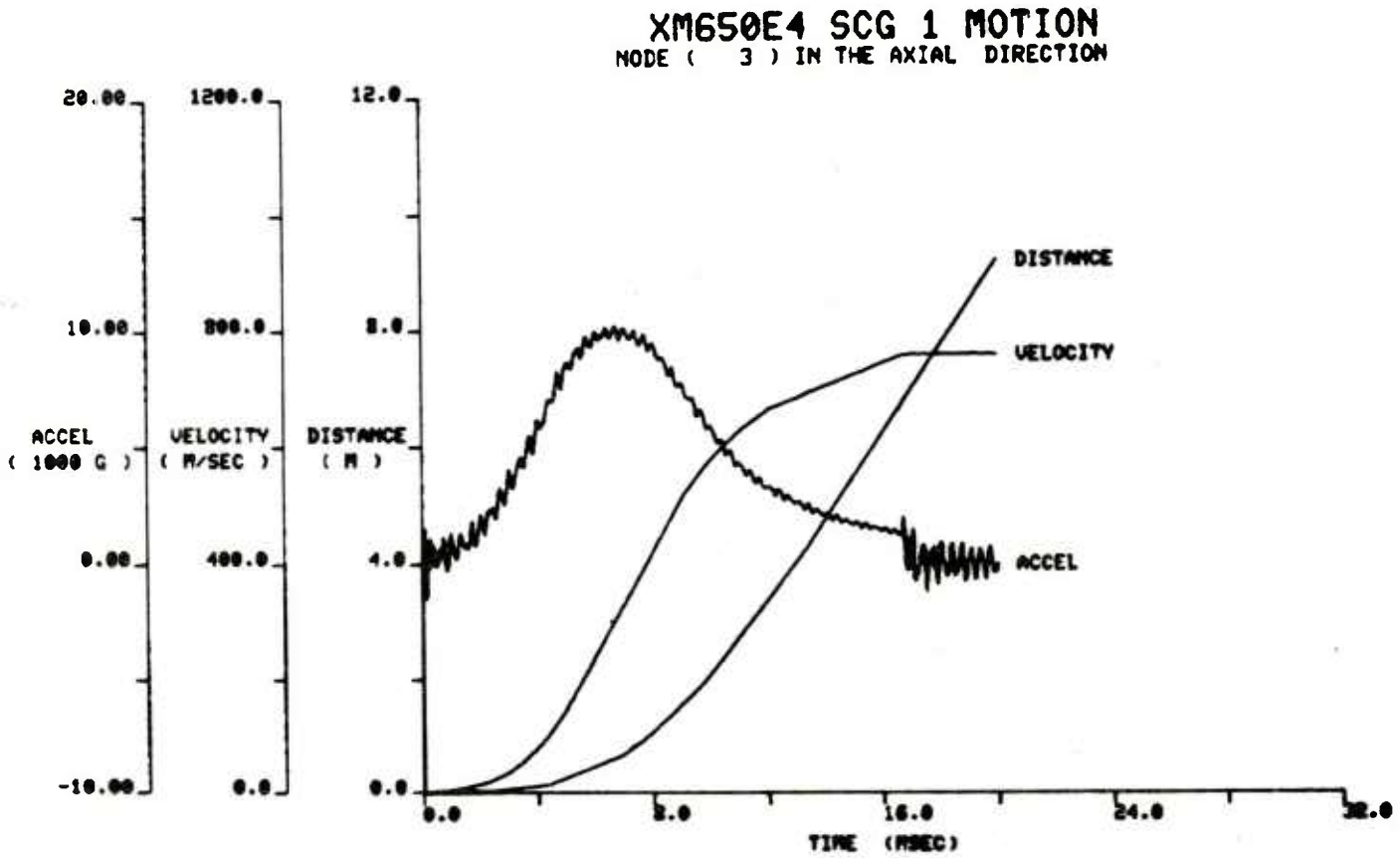

Fig 11 Boat tail motion characteristics for Case 1

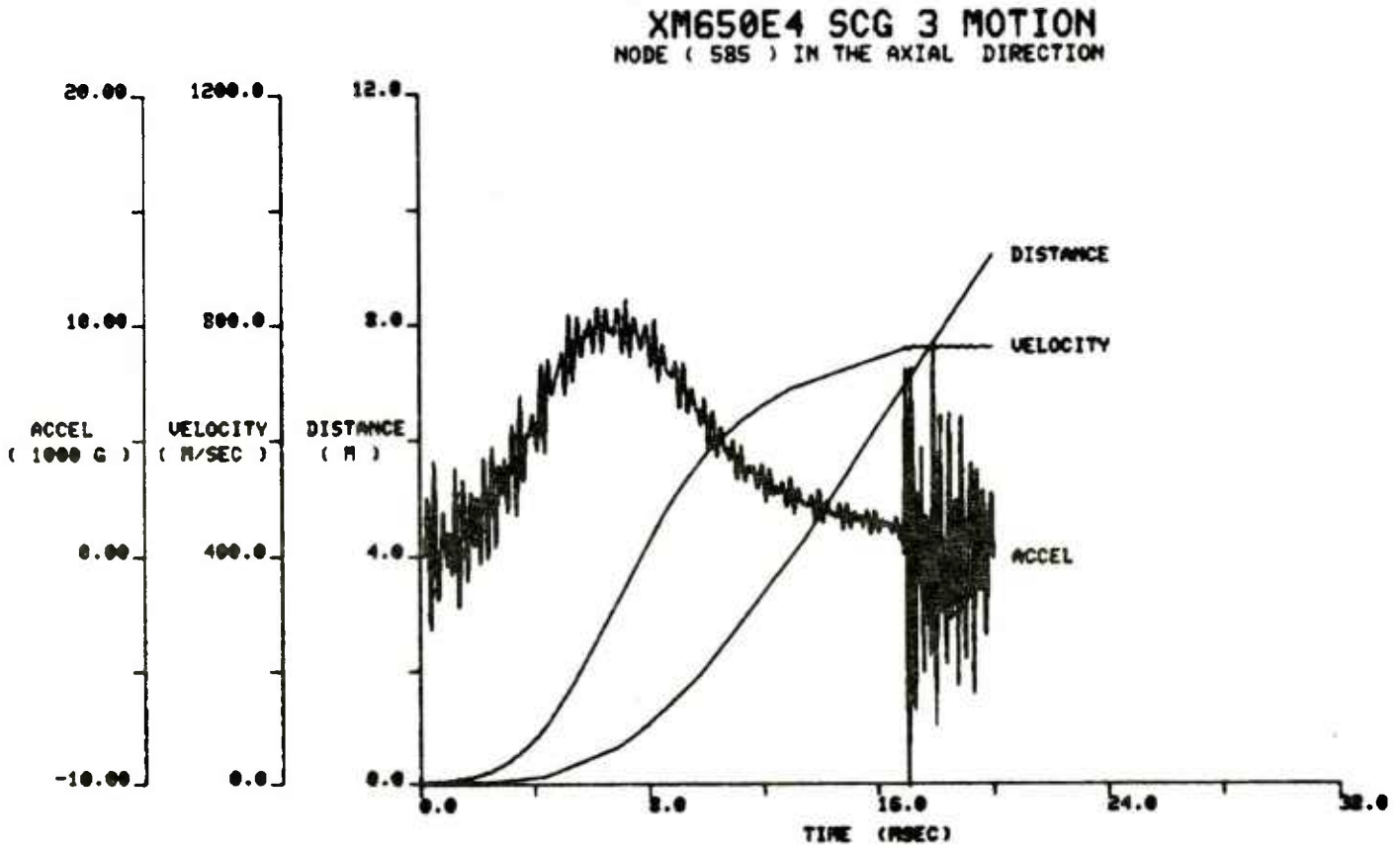

Fig 12 Fuze motion characteristics for Case 3

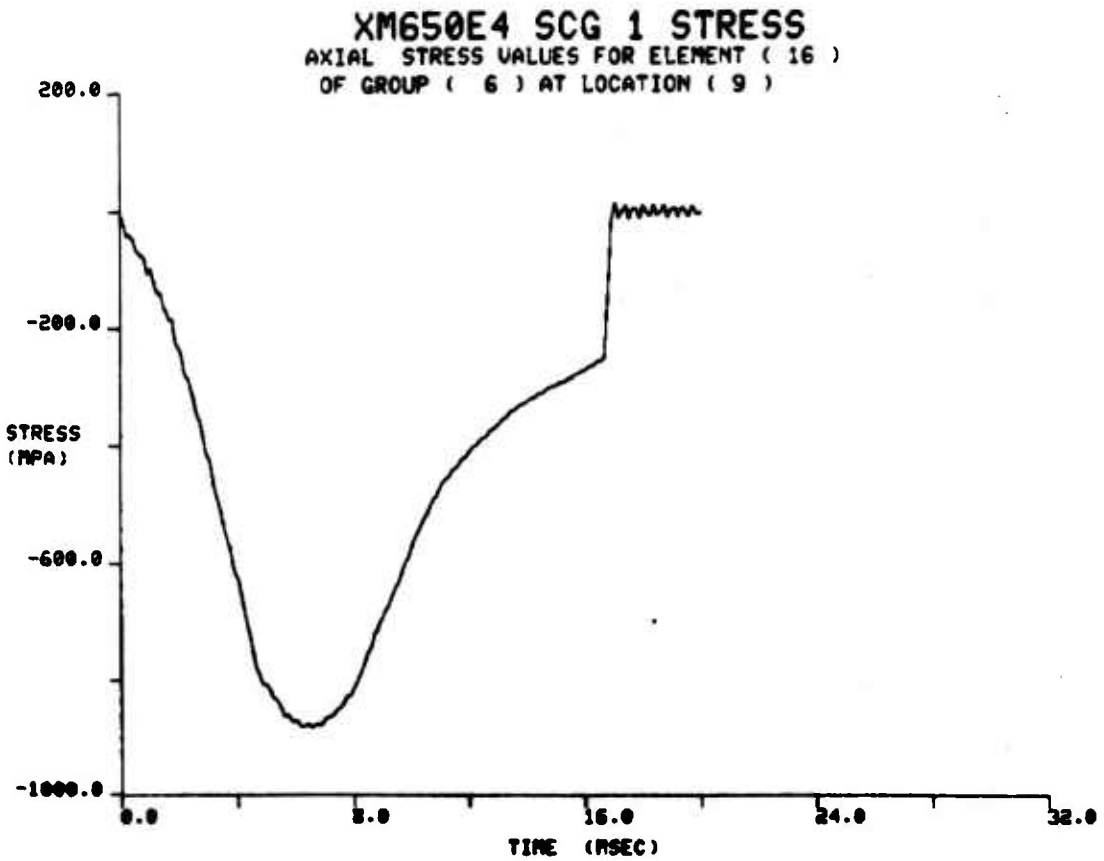

Fig 13 Axial stress variation for rotating band seat element

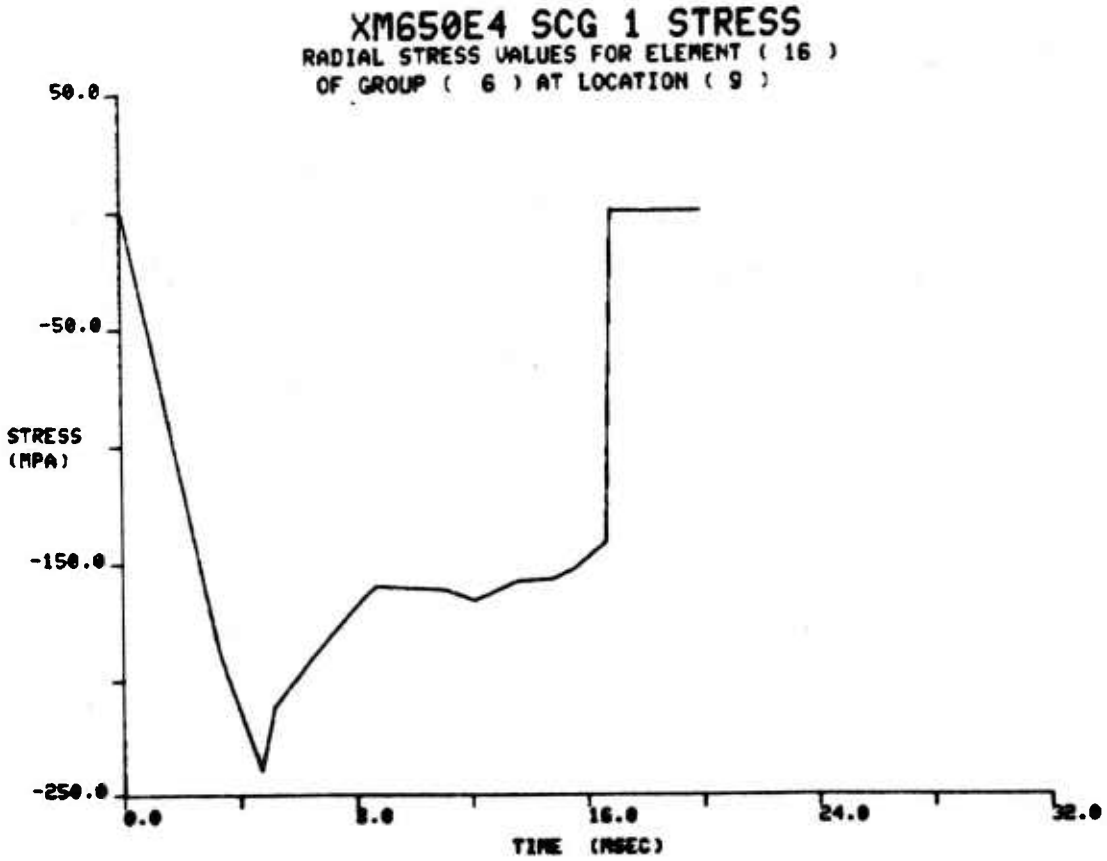

Fig 14 Radial stress variation for rotating band seat element

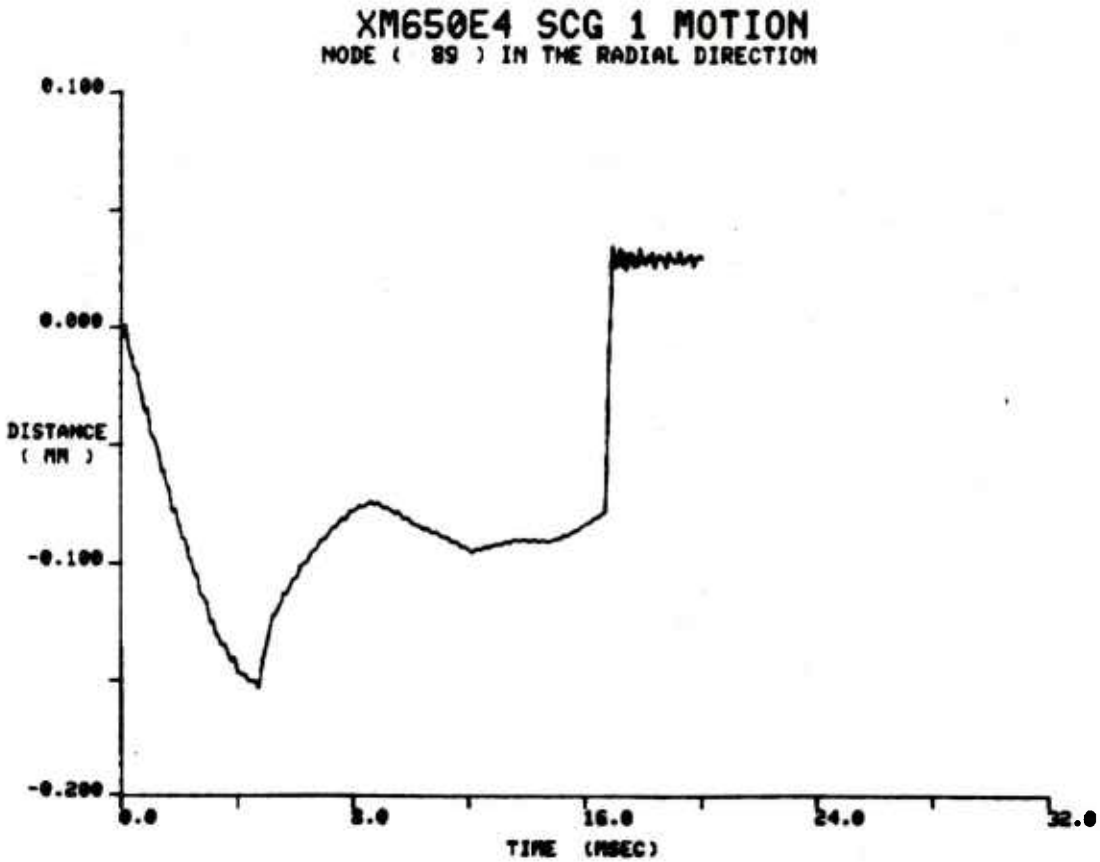

Fig 15 Radial deformation for a band seat node

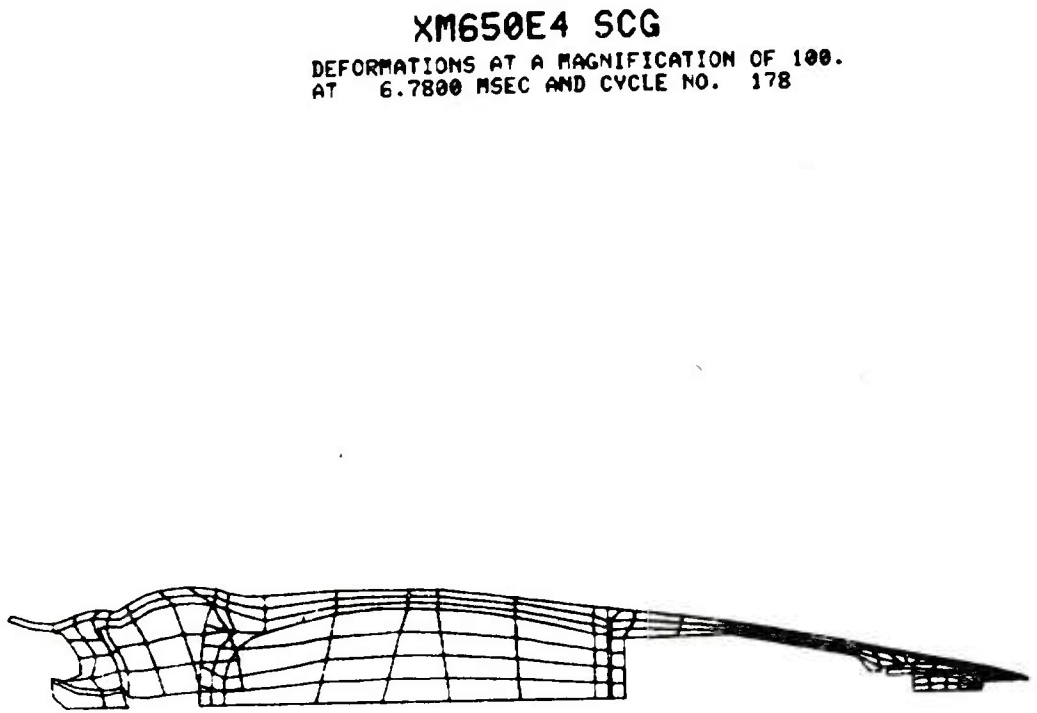

Fig 16 Deformation profile at peak gas pressure

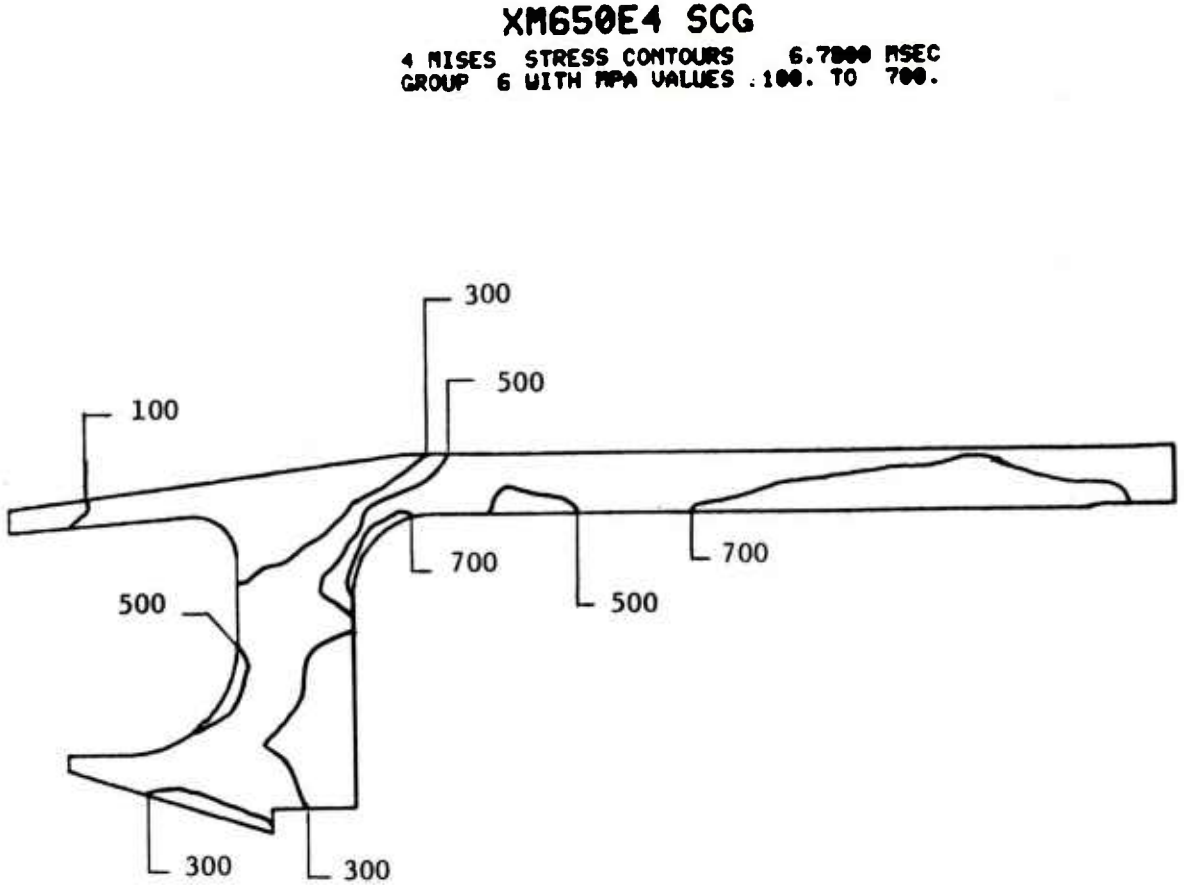

Fig 17 Combined stresses for motor body at peak gas pressure

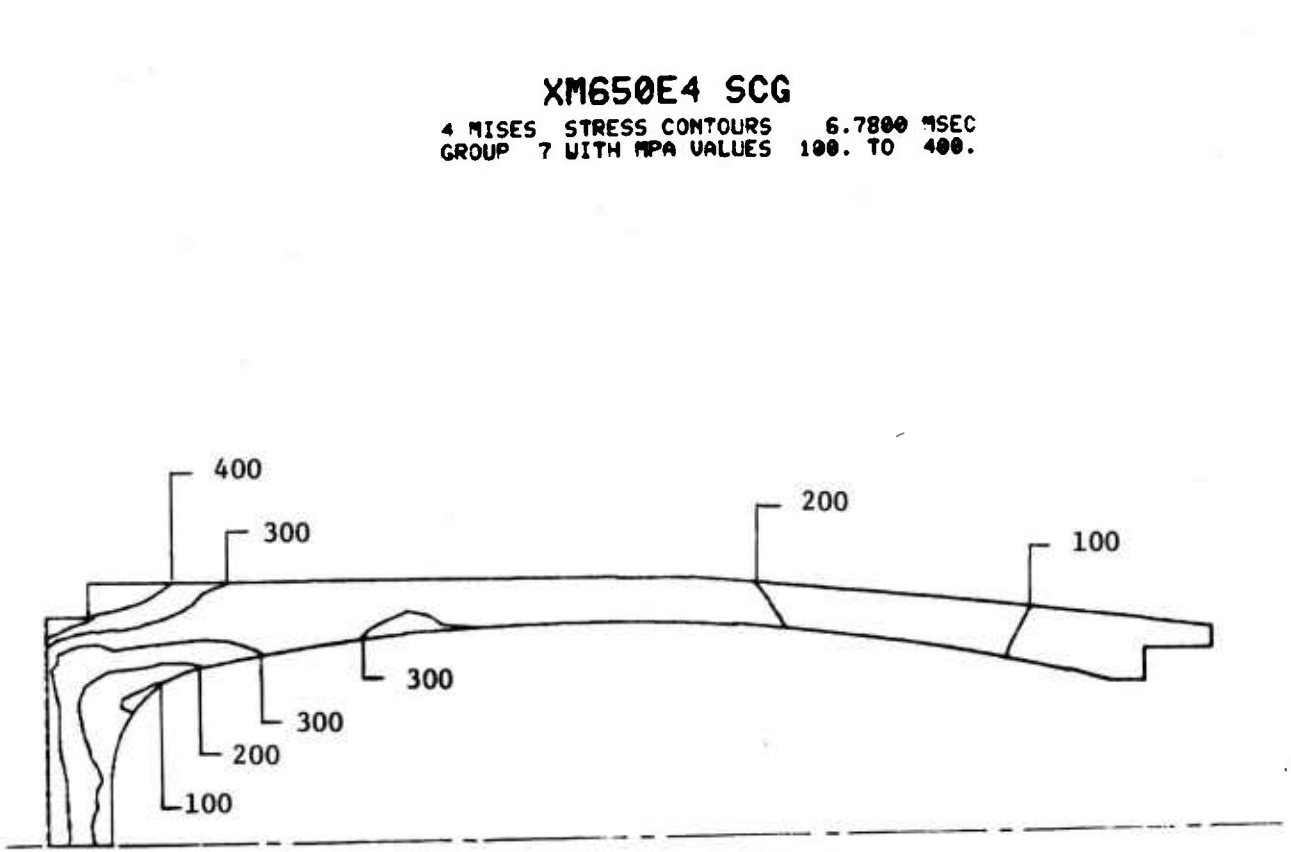

Fig 18 Combined stresses for warhead at peak gas pressure

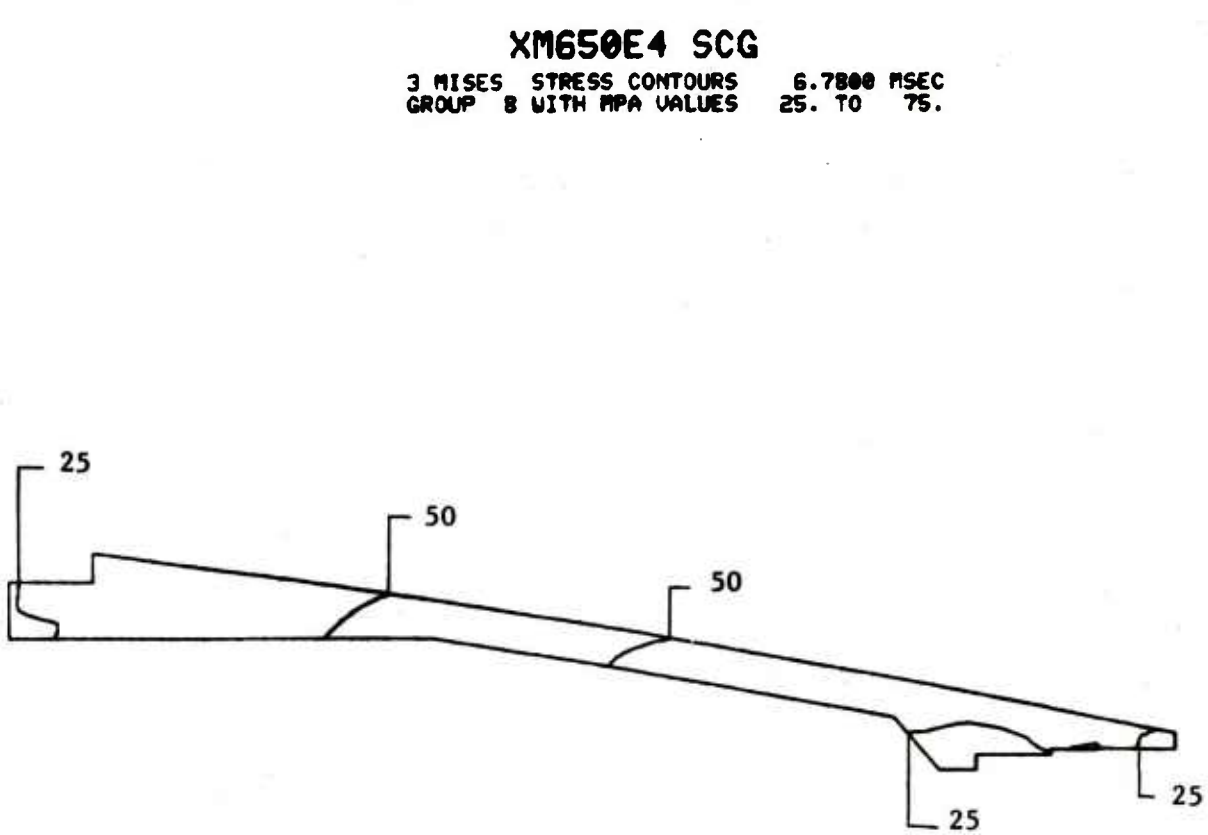

Fig 19 Combined stresses for ogive at peak gas pressure

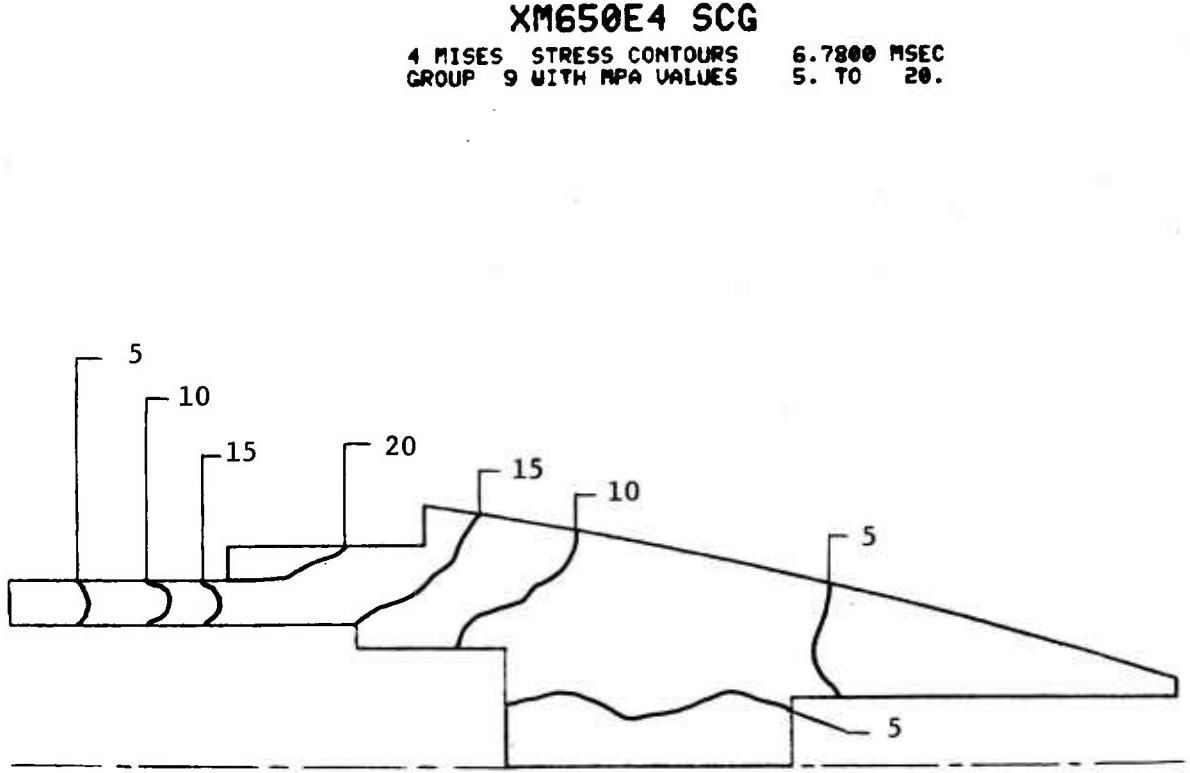

Fig 20 Combined stresses for fuze at peak gas pressure

DISTRIBUTION LIST

Director
Defense Research and Engineering
ATTN: Technical Library
Washington, DC 20301

Commander
Defense Documentation Center
ATTN: DDC-TCA (12)
Cameron Station
Alexandria, VA 22314

Director
Lawrence Livermore Laboratory
ATTN: Dr. G. L. Goudreau
Dr. Roger Werne
P.O. Box 808
Livermore, CA 94550

Director
Los Alamos Scientific Laboratory
ATTN: Dr. R. L. Peeters
Dr. Richard Browning
P.O. Box 1663
Los Alamos, NM 87544

Vice President
Sandia Laboratories
ATTN: Dr. G. A. Benedetti, B122
Dr. M. L. Callabresi, B122
P.O. Box 969
Livermore, CA 94550

Weapon System Concept Team/CSL
ATTN: DRDAR-ACW
Aberdeen Proving Ground, MD 21010

Technical Library
ATTN: DRDAR-CLJ-L
Aberdeen Proving Ground, MD 21010

Technical Library
ATTN: DRDAR-TSB-S
Aberdeen Proving Ground, MD 21005

Benet Weapons Laboratory
Technical Library
ATTN: DRDAR-LCB-TL
Watervliet, NY 12189

Commander
US Army Armament Materiel & Readiness Command
ATTN: DRSAR-LEP-L
Rock Island, IL 61299

Director
US Army TRADOC Systems Analysis Activity
ATTN: ATAA-SL (Technical Library)
White Sands Missile Range, NM 88002

Commander
US Army Armament Research & Development Command
ATTN: DRDAR-TD, Dr. R. Weigle
DRDAR-BLP, Mr. L. A. Watermeier
Mr. S. S. Lentz
Dr. I. W. May
Dr. B. P. Burns
DRDAR-BLT, Dr. J. M. Santiago
DRDAR-LC, Dr. J. Frasier
DRDAR-LCA, Mr. W. Benson
Dr. H. Fair
Mr. L. Rosendorf (10)
DRDAR-LCB, Dr. R. Montgomery
Dr. T. Simkins
DRDAR-LCE, Dr. D. A. Wiegand
Mr. W. E. Voreck
DRDAR-LCF, Mr. F. Saxe
Mr. G. Demitrack
DRDAR-LCM, Mr. S. Kaplowitz
DRDAR-LCN, COL G. Lubold
Mr. J. Drake
Mr. C. J. Spinelli
Mr. S. DiDomenico

DRDAR-LCN, Mr. F. Scerbo
Dr. A. E. Schmidlin
DRDAR-LCS, Mr. J. Gregorits
Mr. R. Corn
DRDAR-LCU, Mr. A. Moss
Mr. G. Jackman
Mr. A. LoPresti
Mr. W. Eppler
Mr. R. Botticelli
Mr. S. Harnett
Mr. V. Ilardi
DRDAR-LCW, Mr. H. Garver
DRDAR-MI, Mr. D. Grobstein
Mr. A. Edwards
Mr. R. Isakower
Mr. B. Barnett
DRDAR-PM, COL R. B. Henry
DRDAR-QA, Mr. D. Adams
DRDAR-SC, Dr. D. Gyorog
Mr. S. Jacobson
DRDAR-SE, COL J. Chesbro
DRDAR-TSS (5)
Dover, NJ 07801

Project Manager
Cannon Artillery Weapon System
ATTN: DRCPM-CAWS, COL Philipp
Dover, NJ 07801

Project Manager
Selected Ammunition
ATTN: DRCPM-SA, COL R. J. Cook, Jr.
Dover, NJ 07801